

### 3.1.5 Xirolimni lagoon

Figures 52-61 show the spatial distribution of Chl-a in Xirolimni lagoon for the years 2013-2021. During 2013 (Figure 55), the first peak is reached in May. The highest values are found at the center of the basin and the southern shores (1.5-2.0  $\mu\text{g/l}$ ). In summer, the northern part exhibits higher values, compared to the rest of the lagoon (up to 3.5  $\mu\text{g/l}$ ). The third peak is reached in November, where higher values are confined at the shores. Then, Chl-a decrease as winter approaches.

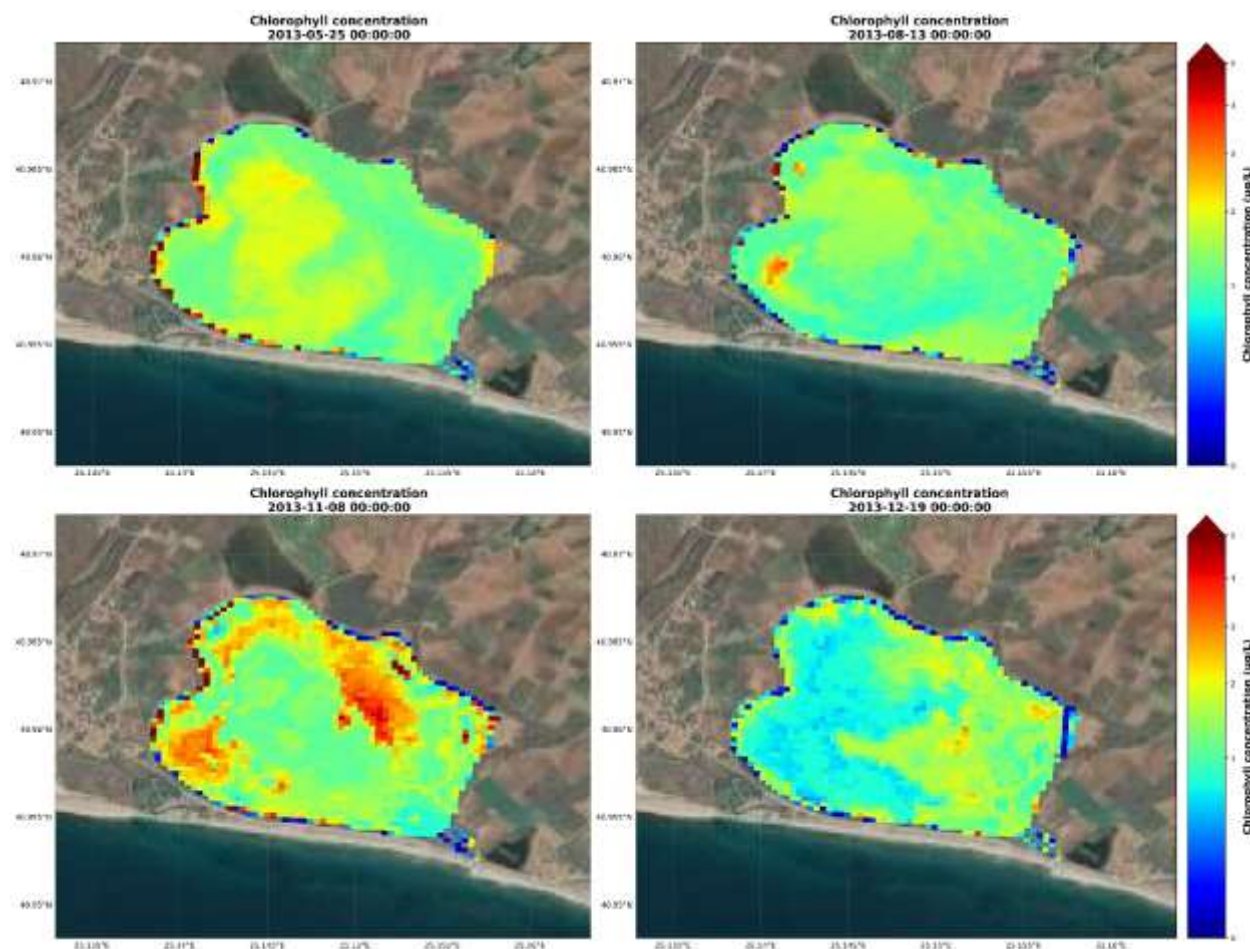


Figure 55. Seasonal evolution of Chl-a concentration in Xirolimni lagoon for the year 2013, based on Landsat 8 satellite images.

Figure 56 illustrates the increase of Chl-a from the beginning of January until the end of summer. Chl-a values in August range from 1.0 to 10  $\mu\text{g/l}$ , with the highest values restricted at the eastern part of the lagoon. In the following months, Chl-a values decrease (1.0-4.0  $\mu\text{g/l}$ ).

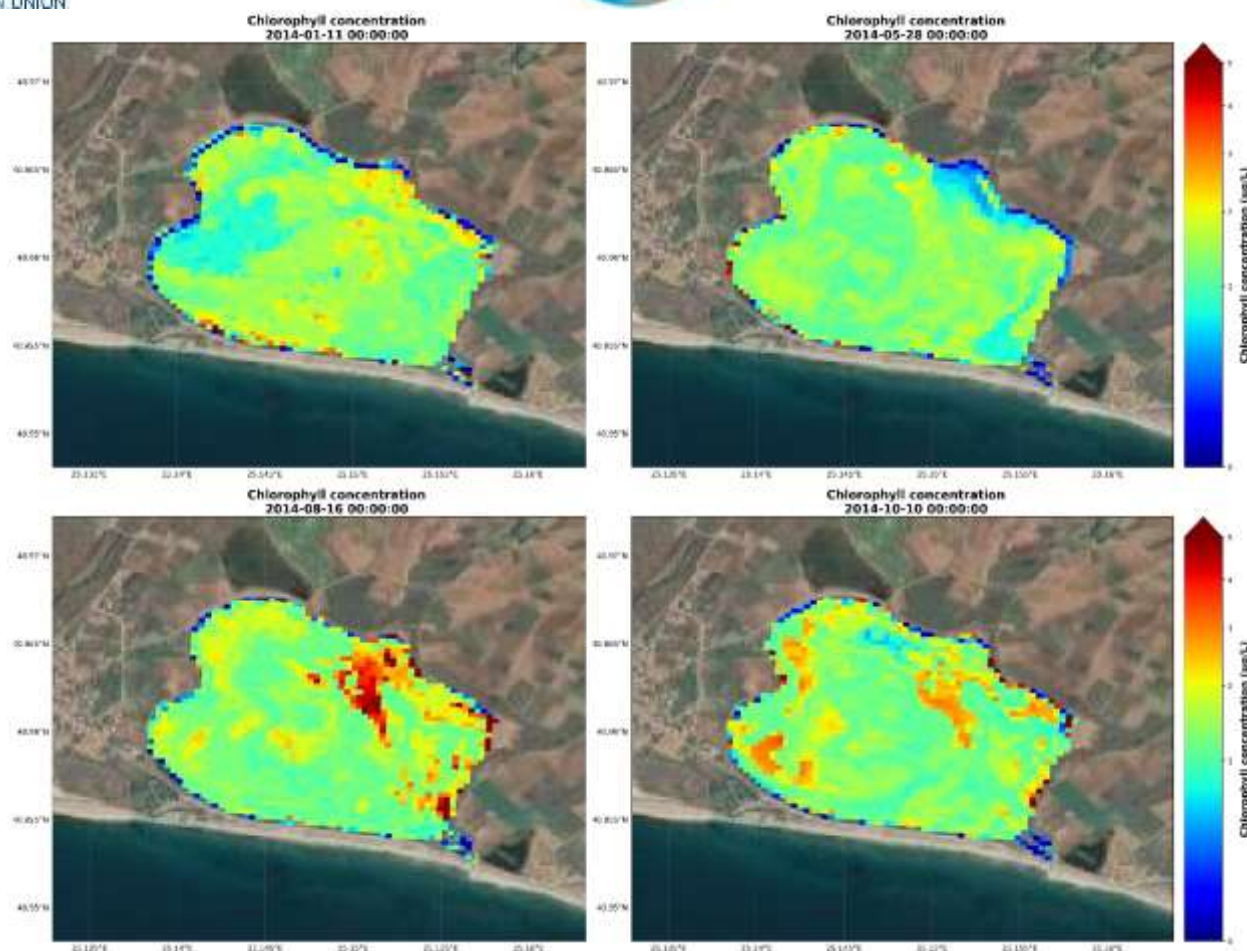


Figure 56. Seasonal evolution of Chl-a concentration in Xirolimni lagoon for the year 2014, based on Landsat 8 satellite images.

The first half of 2015 is presented in Figure 57 covered by Landsat 8 and the second half is presented in Figure 58 covered by Sentinel 2. The images selected for the first half of 2015 show the increase from low Chl-a in February to higher values in June. These higher values in June reach up to 5  $\mu\text{g/l}$ , mostly restricted at the northern and western shores.

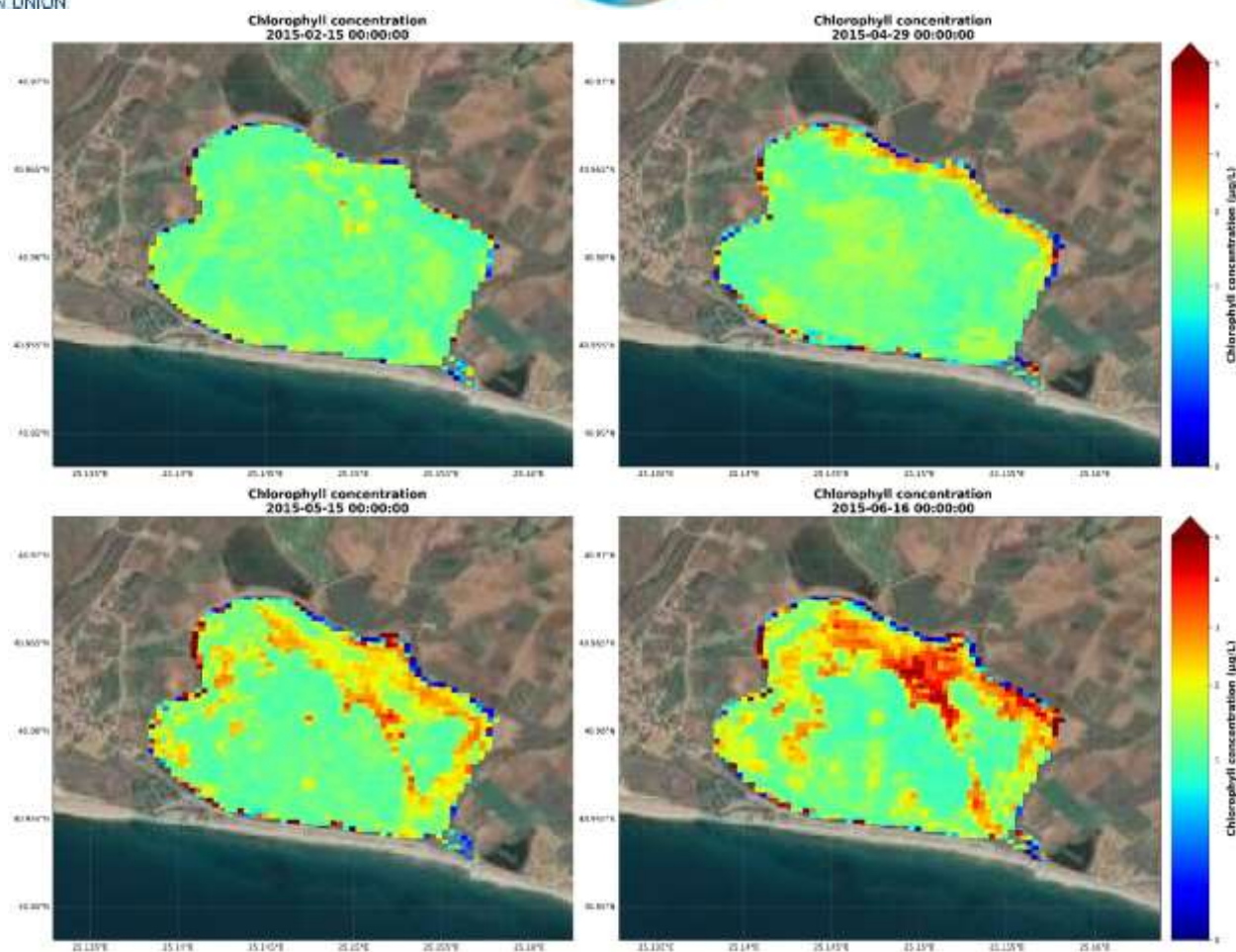


Figure 57. Seasonal evolution of Chl-a concentration in Xirolimni lagoon for the year 2015, based on Landsat 8 satellite images.

In July (Figure 58), Chl-a is almost uniformly distributed across the basin (3.0-5.0 µg/l). From August to November, Chl-a is almost stable, with the higher values concentrated close to the shores.

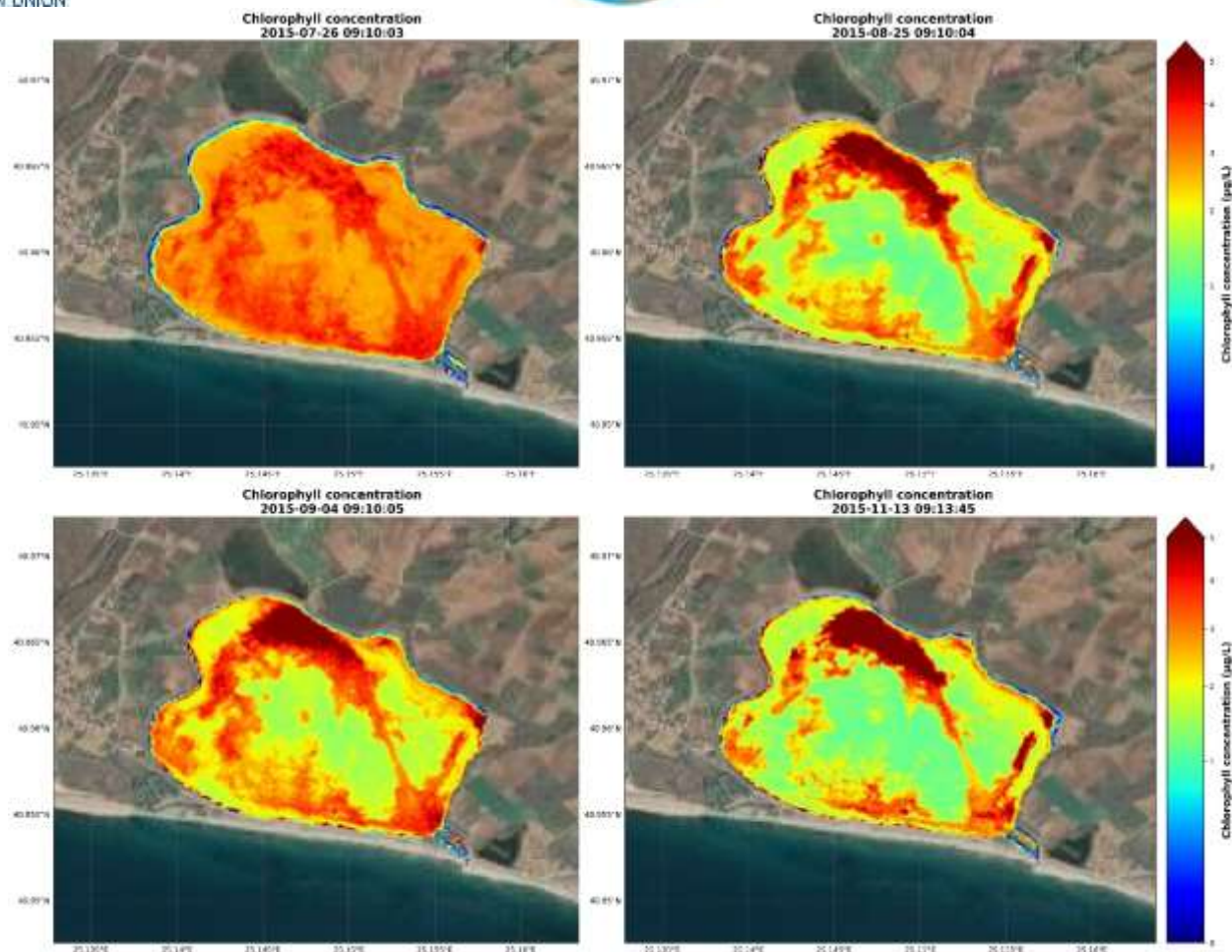


Figure 58. Seasonal evolution of Chl-a concentration in Xirolimni lagoon for the year 2015, based on Sentinel 2 satellite images.

For 2016 three images during summer are presented as due to cloudiness limited images were available covering the seasonal Chl-a cycle (Figure 59). In the first image of July, lower Chl-a values are observed in the center of the basin ( $1.5 \mu\text{g/l}$ ) and the higher values close to the shores (up to  $7.0 \mu\text{g/l}$ ). In the second image of July, Chl-a values increase and they are evenly distributed across the basin. In August, Chl-a decreases but remains evenly distributed.

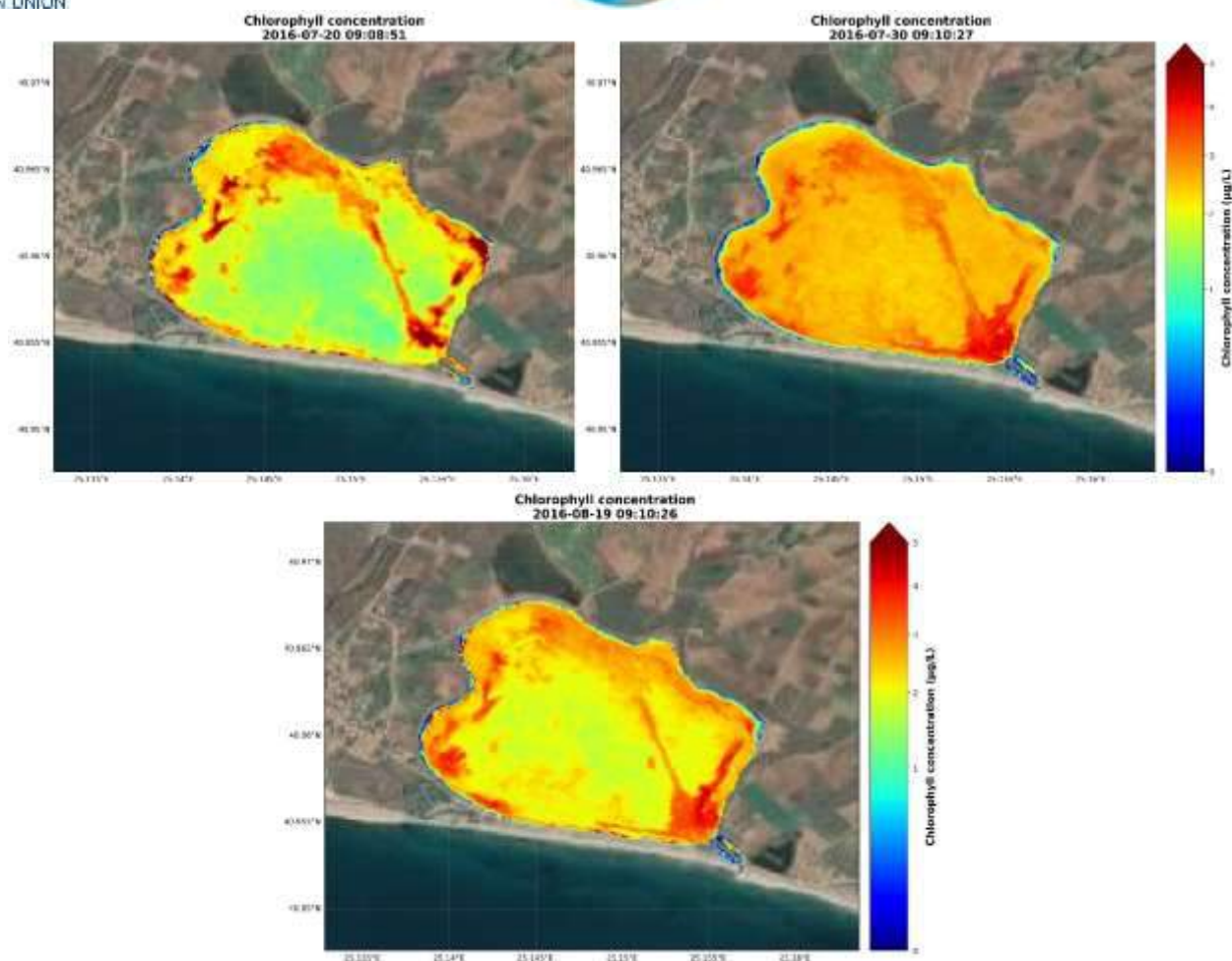


Figure 59. Seasonal evolution of Chl-a concentration in Xiolimni lagoon for the year 2016, based on Sentinel 2 satellite images.

During 2017 (Figure 60), higher Chl-a values are observed close to the shores of the lagoon. These increased values move towards the central part in April and then expand to the whole basin in May. The highest Chl-a reaches 55 µg/l in May. In the following months, Chl-a decreases to its lowest values in December (1.3-4.0 µg/l).

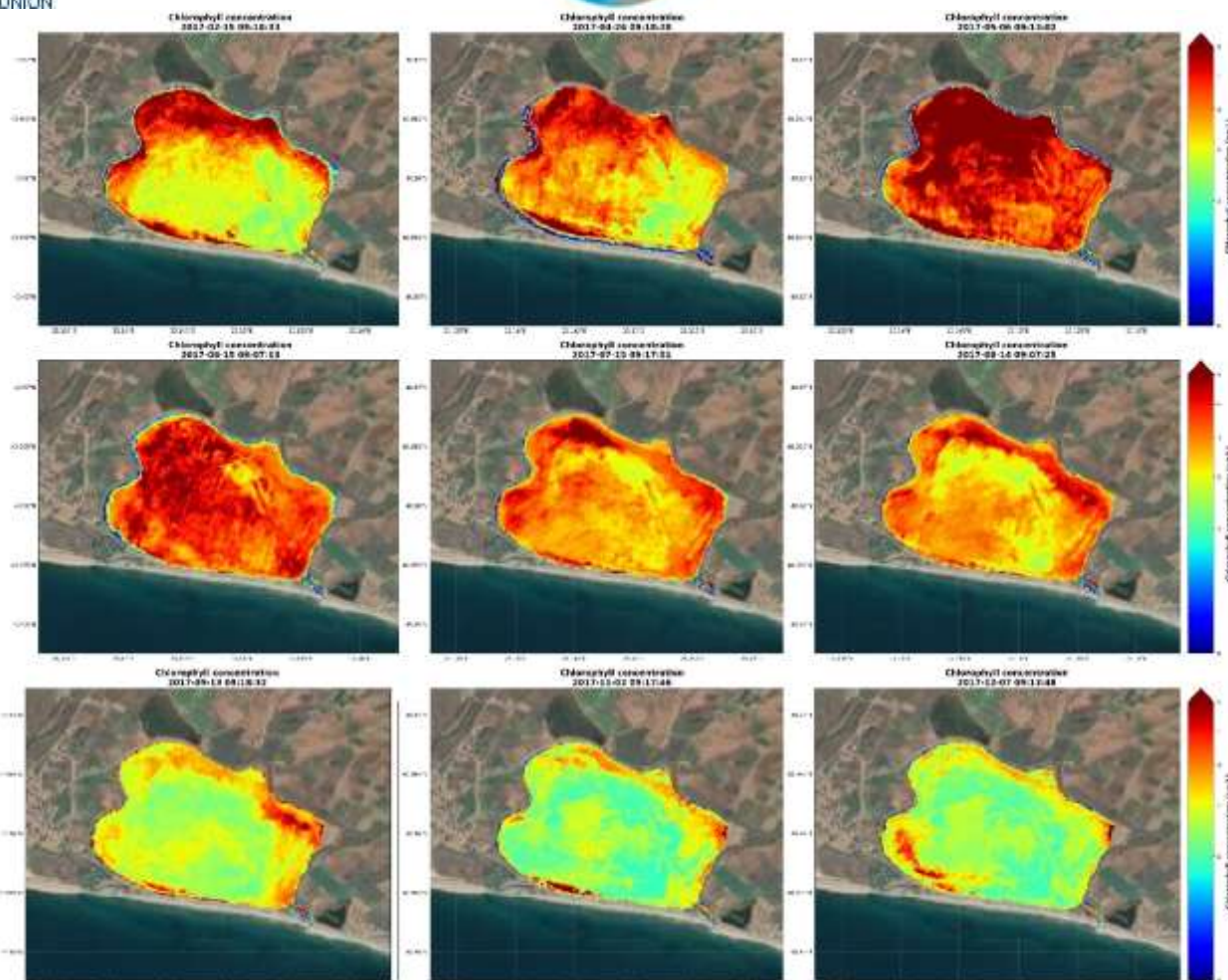


Figure 60. Seasonal evolution of Chl-a concentration in Xirolimni lagoon for the year 2017, based on Sentinel 2 satellite images.

Figure 61 shows the increase of Chl-a values, from low concentrations in January to higher in May. Almost the whole basin shows high Chl-a values that range from 2.5 to 8.0  $\mu\text{g/l}$ . In June, Chl-a values decrease at the northern part (lower than 1.5  $\mu\text{g/l}$ ), but increase at the southern and eastern shores. In the following months, Chl-a decreases until its lowest values, by the end of July. A peak is observed in mid-August, with higher values concentrating in the center and close to the shores of the lagoon. Another peak is observed in November, where Chl-a ranges from 2.5 to 7  $\mu\text{g/l}$ .

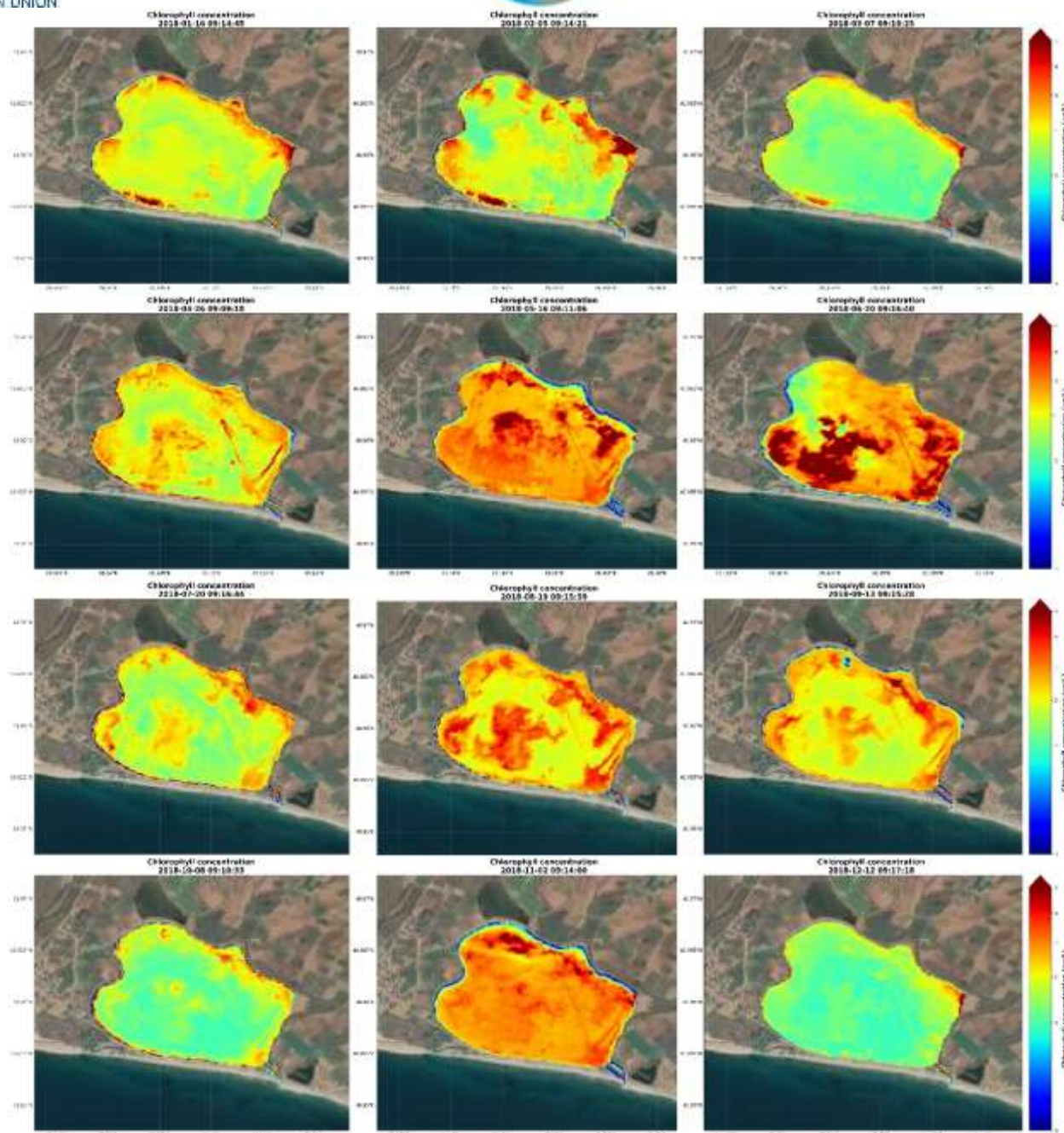


Figure 61. Seasonal evolution of Chl-a concentration in Xirolimni lagoon for the year 2018, based on Sentinel 2 satellite images.

During 2019 (Figure 62), Chl-a starts to increase until late April, reaching the first peak. Chl-a appears evenly distributed across the basin, ranging from 2.5 to 3.5  $\mu\text{g/l}$ . In the following months, Chl-a values decrease, with the higher values moving towards the shores. In November, a maximum is reached which remains stable until December.

The high values detected in December 2019 led to high values in January 2020 (Figure 63). Higher values are met across the shores (up to 5.0  $\mu\text{g/l}$ ) and lower at the central parts of the

basin ( $1.5 \mu\text{g/l}$ ). The first Chl-a peak is observed in May. Chl-a values increase from February and reach the highest values in May. Then Chl-a decreases until November. In mid-November, a maximum is reached ( $2.5\text{-}3.5 \mu\text{g/l}$ ).

During 2021 (Figure 64), a maximum in Chl-a values is reached in July with the higher values are mostly found at the northern and southern parts. The increase spreads from the northern shores to the central basin (March to June 2021). In the following months, a decrease is observed in the autumn and winter months.

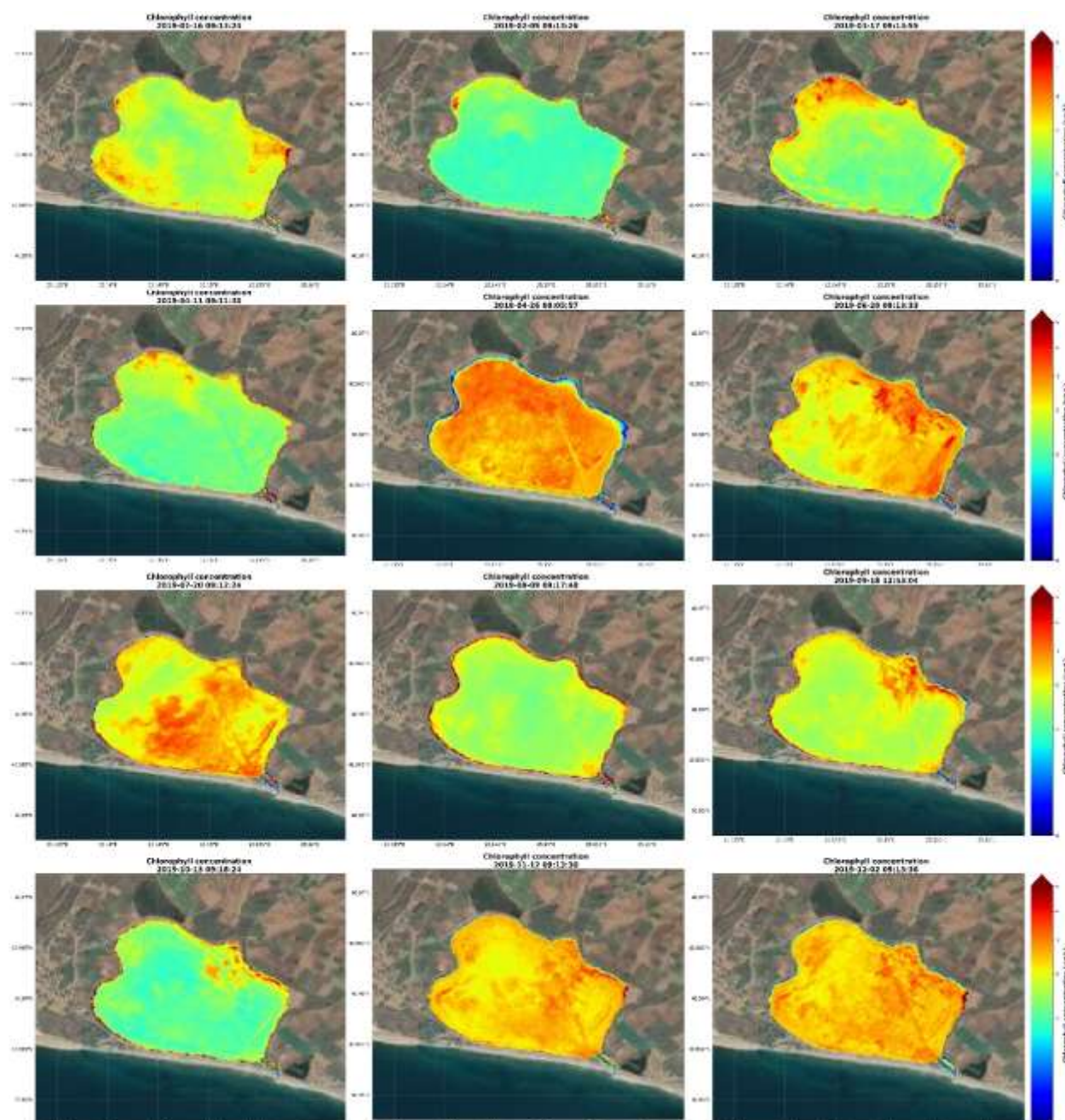


Figure 62. Seasonal evolution of Chl-a concentration in Xirolimni lagoon for the year 2019, based on Sentinel 2 satellite images.

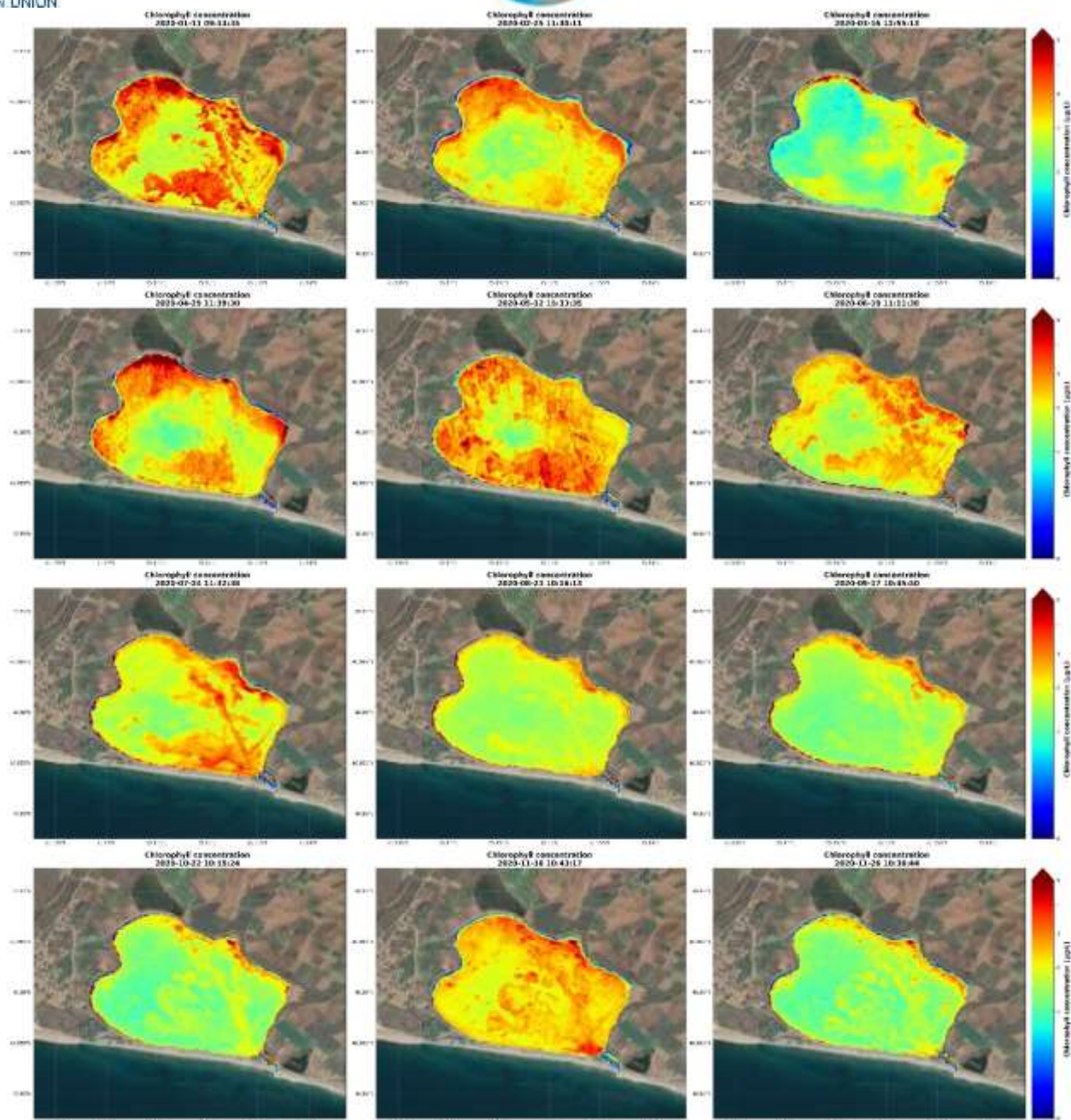


Figure 63. Seasonal evolution of Chl-a concentration in Xirolimni lagoon for the year 2020, based on Sentinel 2 satellite images.

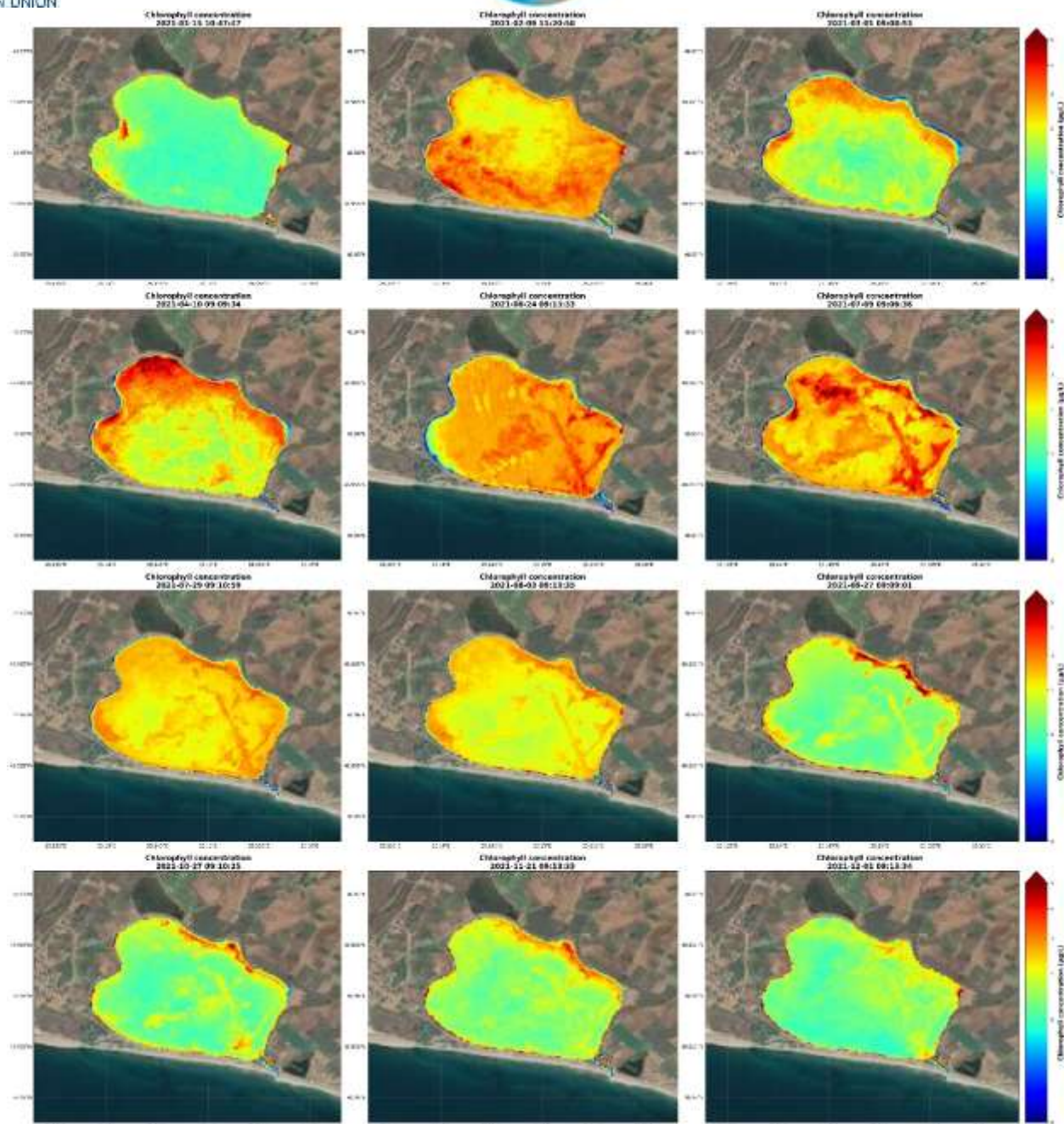


Figure 64. Seasonal evolution of Chl-a concentration in Xiolimni lagoon for the year 2021, based on Sentinel 2 satellite images.

### 3.1.6 Ptelea lagoon

Figures 62-71 present the spatial distribution of Chl-a in Ptelea lagoon for the years 2013-2021. During 2013 (Figure 65), the first peak is reached in May. The highest values are mostly concentrated at the eastern shores (up to 30  $\mu\text{g/l}$ ) and the northern part of the basin (3.0-3.5  $\mu\text{g/l}$ ). In the following months, Chl-a decreases until July, when it starts to increase again until late summer. This concentration rise starts from the northern part (July, 2.5-3.0  $\mu\text{g/l}$ ) and eventually is transferred at the center of the basin (late August). In summer, the eastern and western shores show high values, ranging from 4.0 to 30  $\mu\text{g/l}$ . The third peak is reached in November and then Chl-a decrease as we move towards the winter.

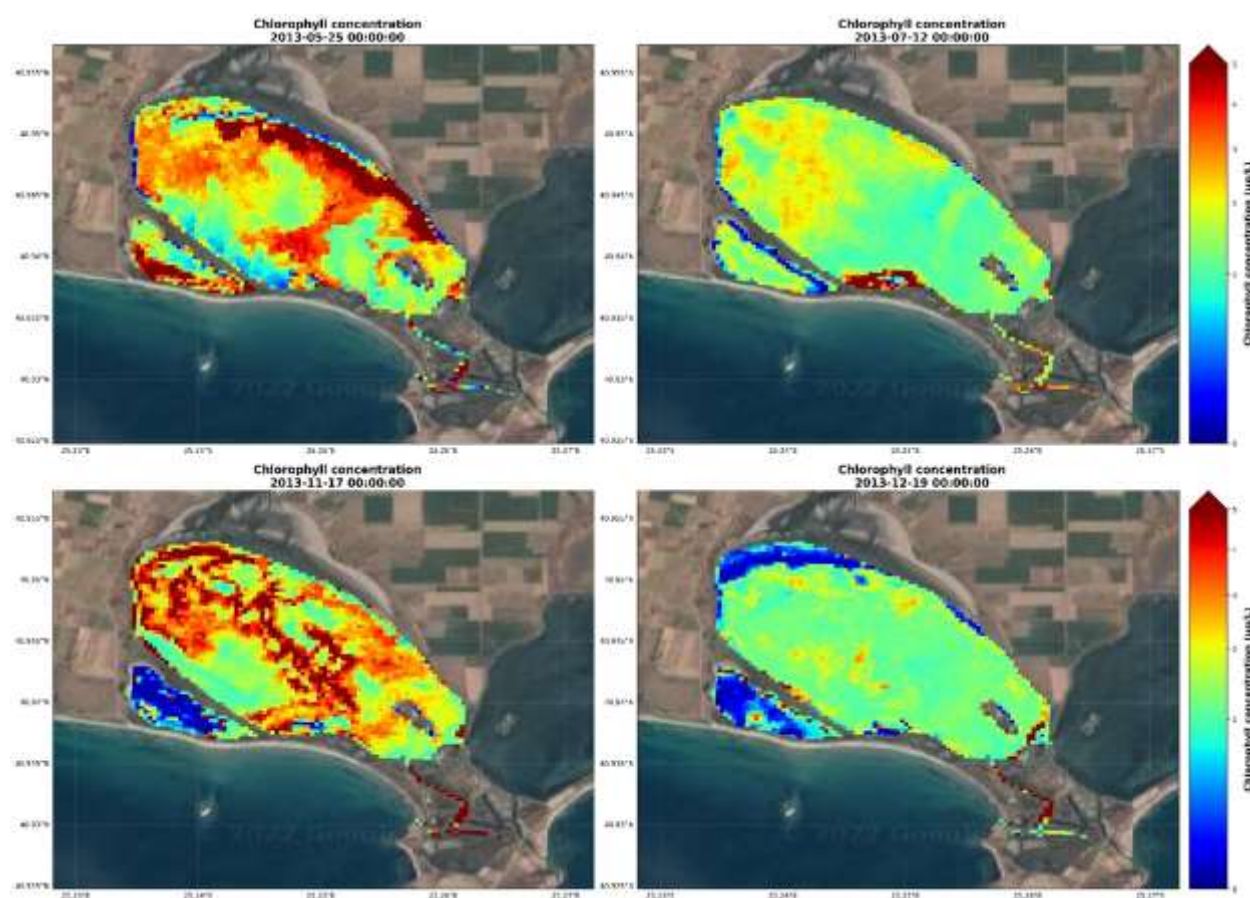


Figure 65. Seasonal evolution of Chl-a concentration in Ptelea lagoon for the year 2013, based on Landsat 8 satellite images.

Figure 66 shows the increase of Chl-a, from low concentrations at the beginning of the year to higher in the summer. Chl-a values range from 1.0 to 3.0  $\mu\text{g/l}$  in late June, with the highest values being detected at the southern parts of the basin. In August, the highest values are found near the northern shores and the north-western shallow parts. In the following months, the high values seem to move towards the center of the lagoon (1.5-2.0  $\mu\text{g/l}$ ).

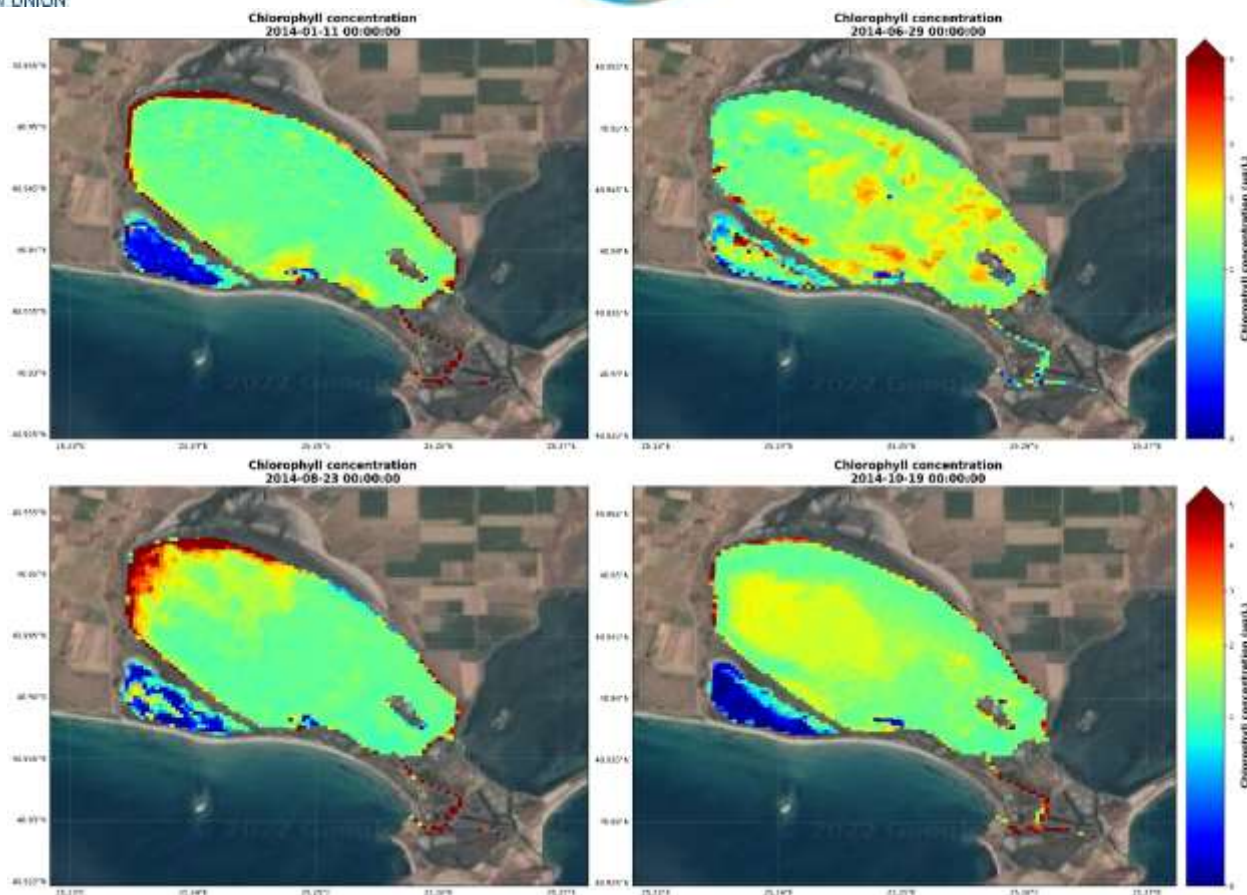


Figure 66. Seasonal evolution of Chl-a concentration in Ptelea lagoon for the year 2014, based on Landsat 8 satellite images.

The first half of 2015 is presented in Figure 67 covered by Landsat 8 and the second half is presented in Figure 68 covered by Sentinel 2. The images selected for the first half of 2015 illustrate that the first peak is reached at the end of spring. In February, Chl-a values range from 0.5 to 1.6  $\mu\text{g/l}$  covering the major parts of the lagoon, with the exception of the northern part, which shows higher values up to 5  $\mu\text{g/l}$ . Increased values spread towards the center of the lagoon in April and covers the whole basin in May.

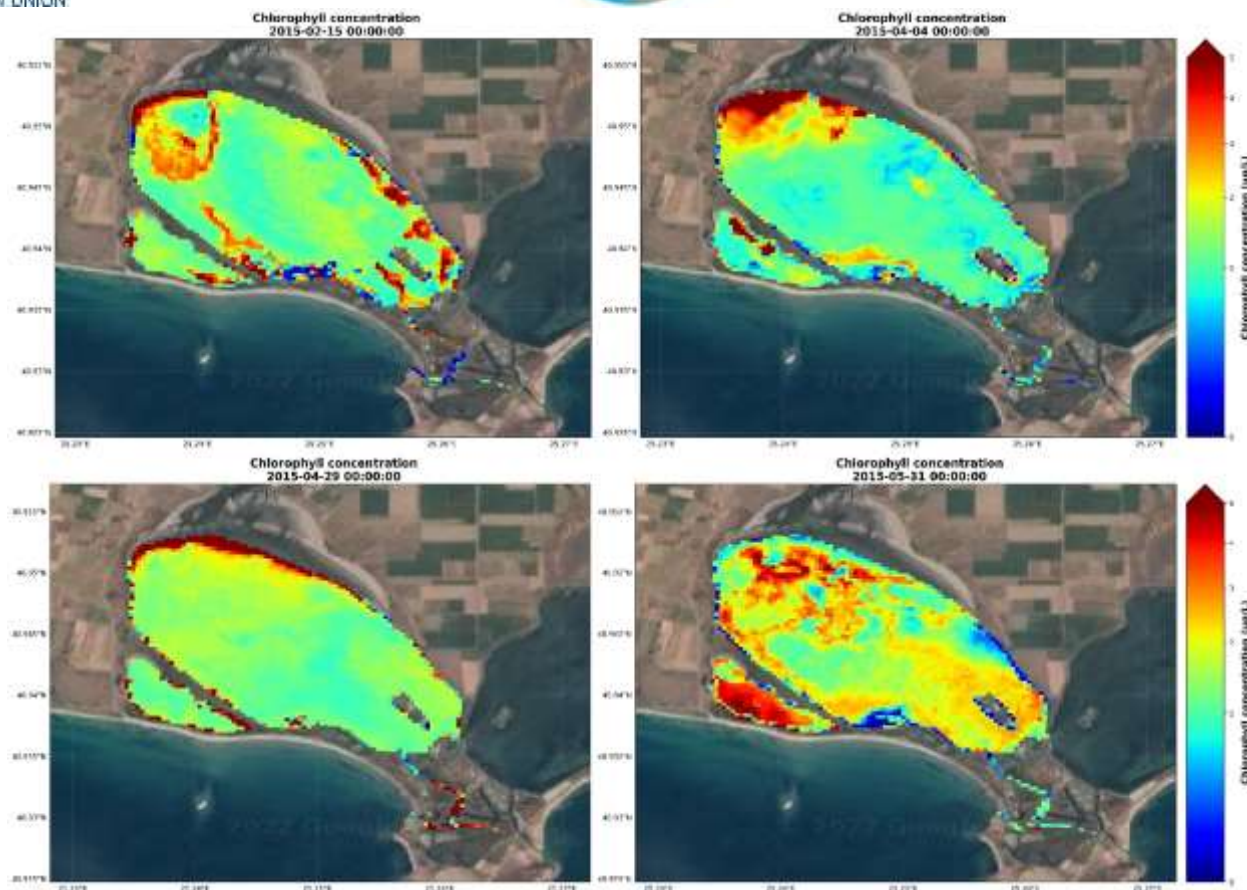


Figure 67. Seasonal evolution of Chl-a concentration in Ptelea lagoon for the year 2015, based on Landsat 8 satellite images.

For the second half of 2015 (Figure 68), higher values are detected at the center of the lagoon during the summer and the first months of autumn (8.0-20.0  $\mu\text{g/l}$ ). Another peak is observed in November, where the Chl-a values at the basin range from 8.0 to 15.0  $\mu\text{g/l}$  and higher values are concentrated at the south-eastern part (30  $\mu\text{g/l}$ ) of the lagoon.

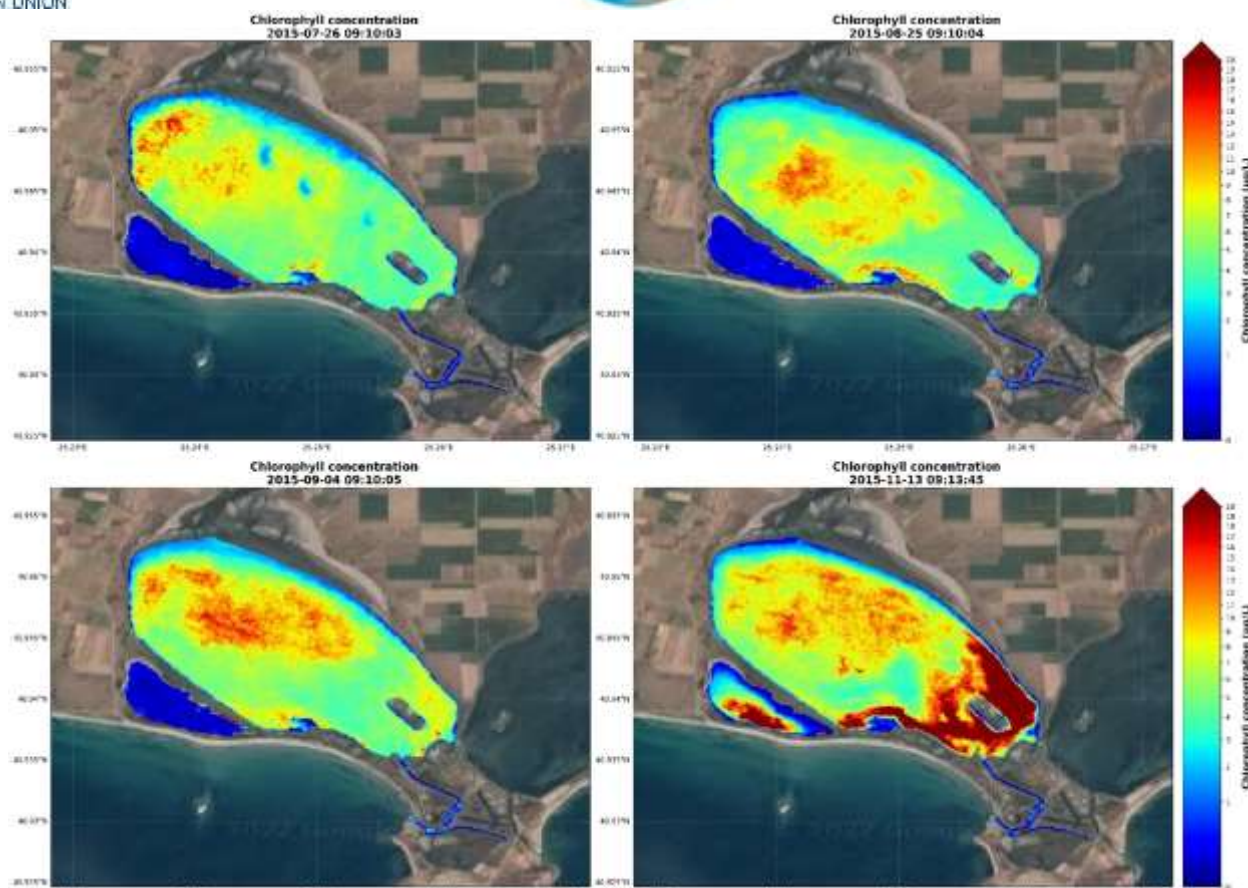


Figure 68. Seasonal evolution of Chl-a concentration in Ptelea lagoon for the year 2015, based on Sentinel 2 satellite images.

For 2016 two images during summer are presented as due to cloudiness these were the only images available for processing (Figure 69). In July, low Chl-a values are observed at the northern part of the lagoon (up to 1.5 µg/l) and higher values on the southern part, reaching 35 µg/l. In August, Chl-a values range around 2 µg/l covering most of the basin, except for the western part where they range from 7.0 to 15.0 µg/l.

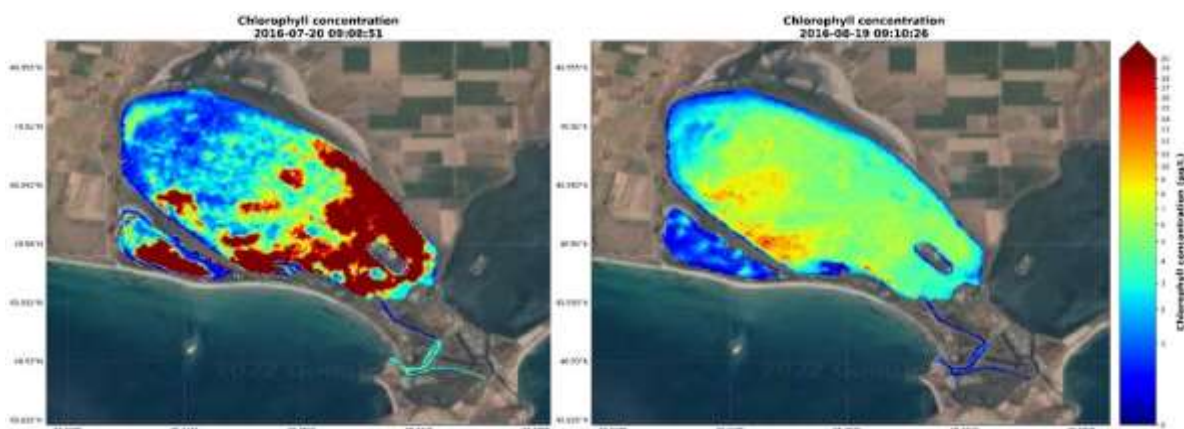


Figure 69. Seasonal evolution of Chl-a concentration in Ptelea lagoon for the year 2016, based on Sentinel 2 satellite images.

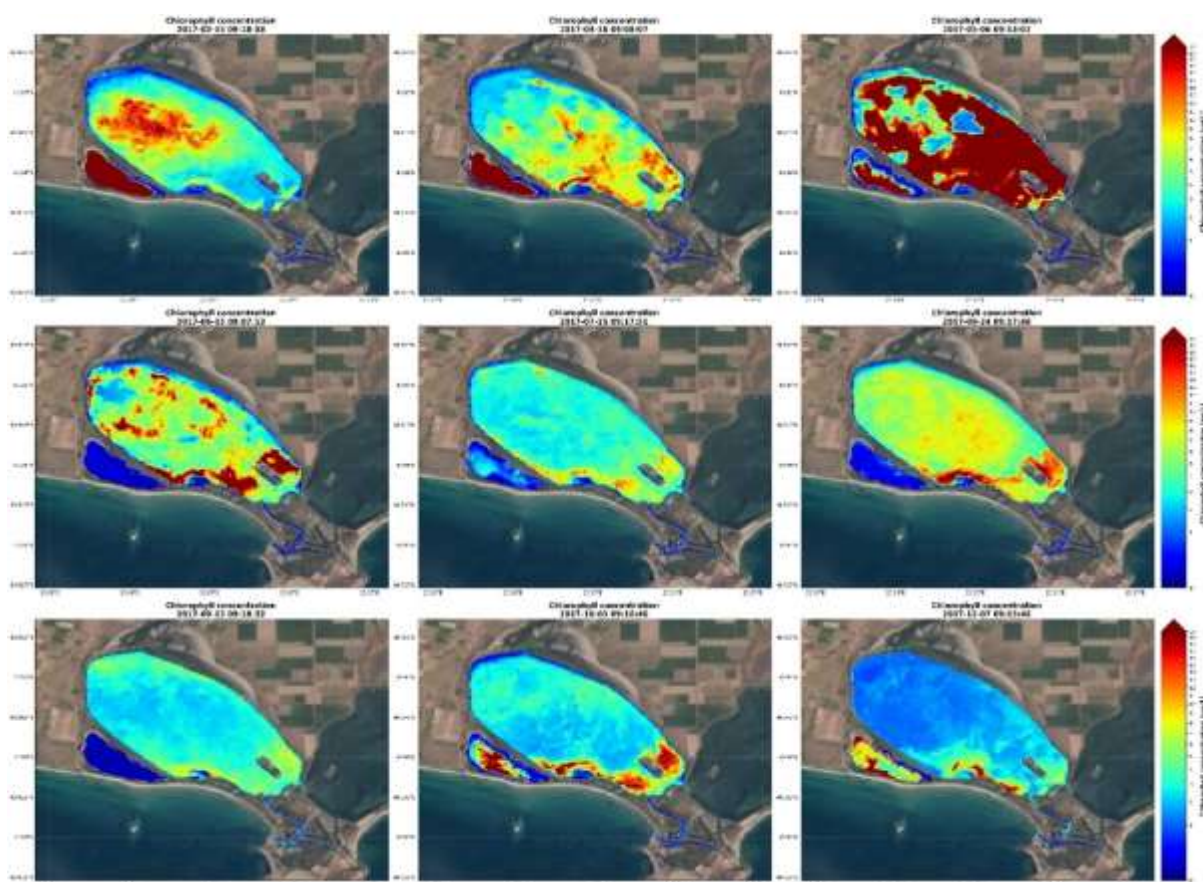


Figure 70. Seasonal evolution of Chl-a concentration in Ptelea lagoon for the year 2017, based on Sentinel 2 satellite images.

During 2017 (Figure 70), higher Chl-a values are observed at the north-western parts of the lagoon (up to 24  $\mu\text{g/l}$ ). These increased values are gradually expanded to the southern parts in April, and eventually cover the whole basin in May. The highest Chl-a reached in May is 40  $\mu\text{g/l}$ . In the following months, Chl-a decreases and the next peak is observed in August. In autumn and winter months the Chl-a values decrease, reaching their minimum values in December.

Figure 71 shows the increase of Chl-a values, from low concentrations in January to higher in late May. Almost the whole basin shows high Chl-a values that exceed 30  $\mu\text{g/l}$ . In the following months, Chl-a decreases, until the lowest values are reached, in the beginning of August. A peak is observed in the first days of September, with higher values concentrating at the center and the western shore of the lagoon. In the autumn and winter months, Chl-a values are decreased throughout the basin.

During 2019 (Figure 72), Chl-a starts to increase in late June. The event begins from the eastern shores and the southern parts and ultimately spreads over the basin in November. Chl-a values decrease gradually in December.

The first Chl-a peak in 2020 (Figure 73) is observed in May. Chl-a values start increasing from February and reach their highest values in May (up to 35  $\mu\text{g/l}$ ). Then, Chl-a decreases until early September. From mid-September, the Chl-a values increase again starting from the northern and southern parts and spreading to the whole basin by November.

Increased Chl-a values are detected in January 2021 (Figure 74) compared to the previous years, reaching 40  $\mu\text{g/l}$ . In the following months, Chl-a values decrease and then increase again during spring. High values are observed in late September, remaining high until November and confine only to the southern part in December.

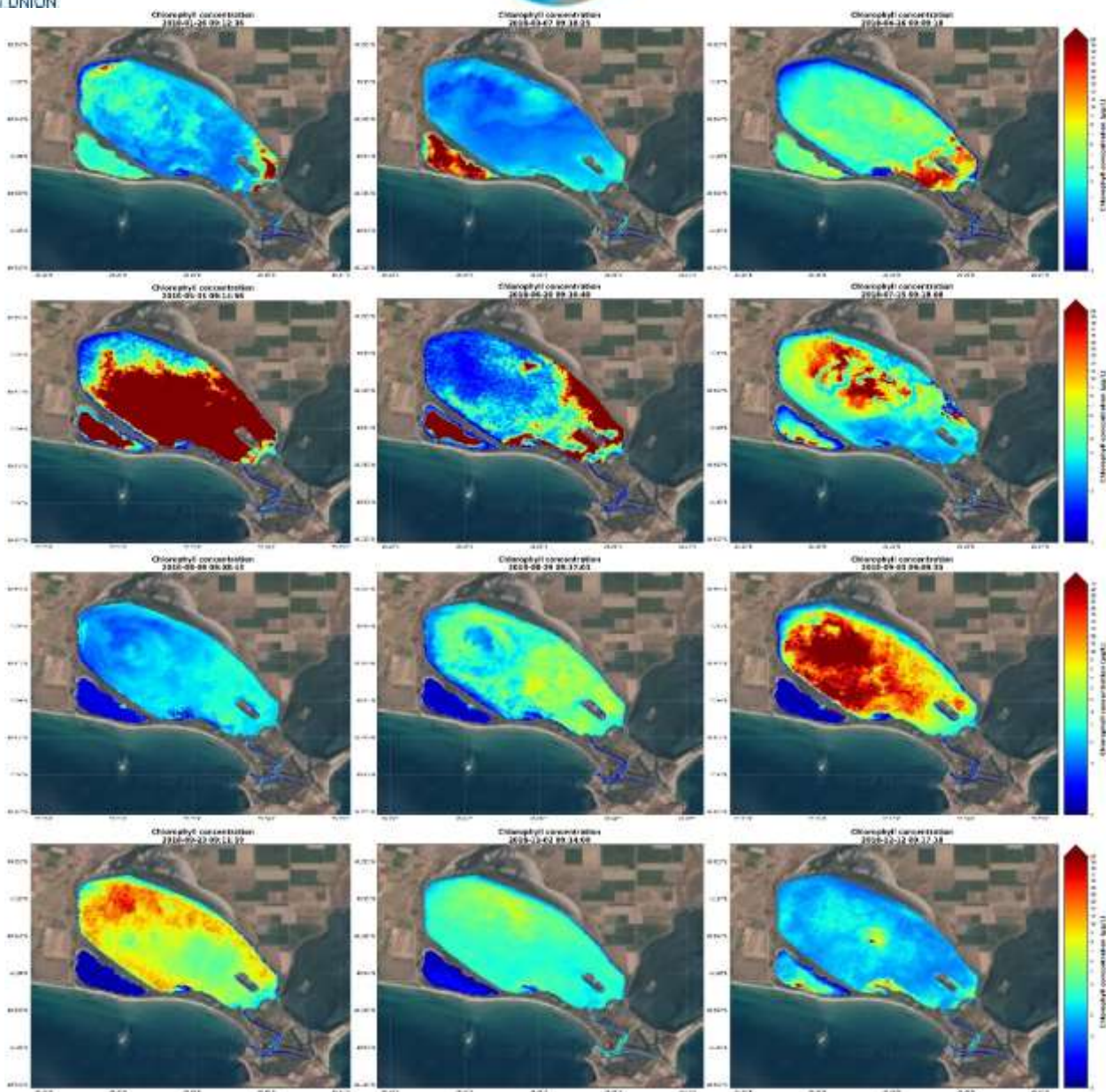


Figure 71. Seasonal evolution of Chl-a concentration in Ptelea lagoon for the year 2018, based on Sentinel 2 satellite images.

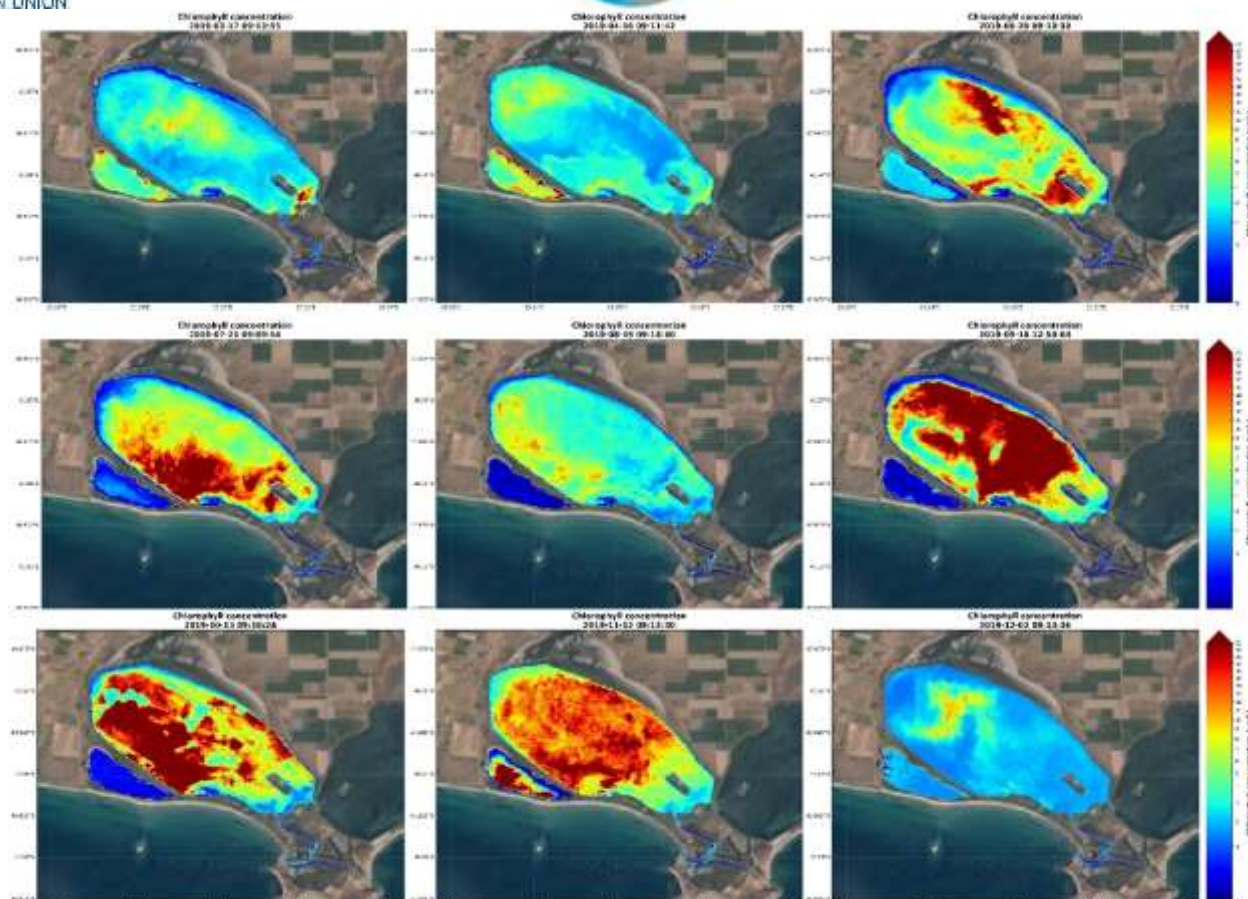


Figure 72. Seasonal evolution of Chl-a concentration in Ptelea lagoon for the year 2019, based on Sentinel 2 satellite images.

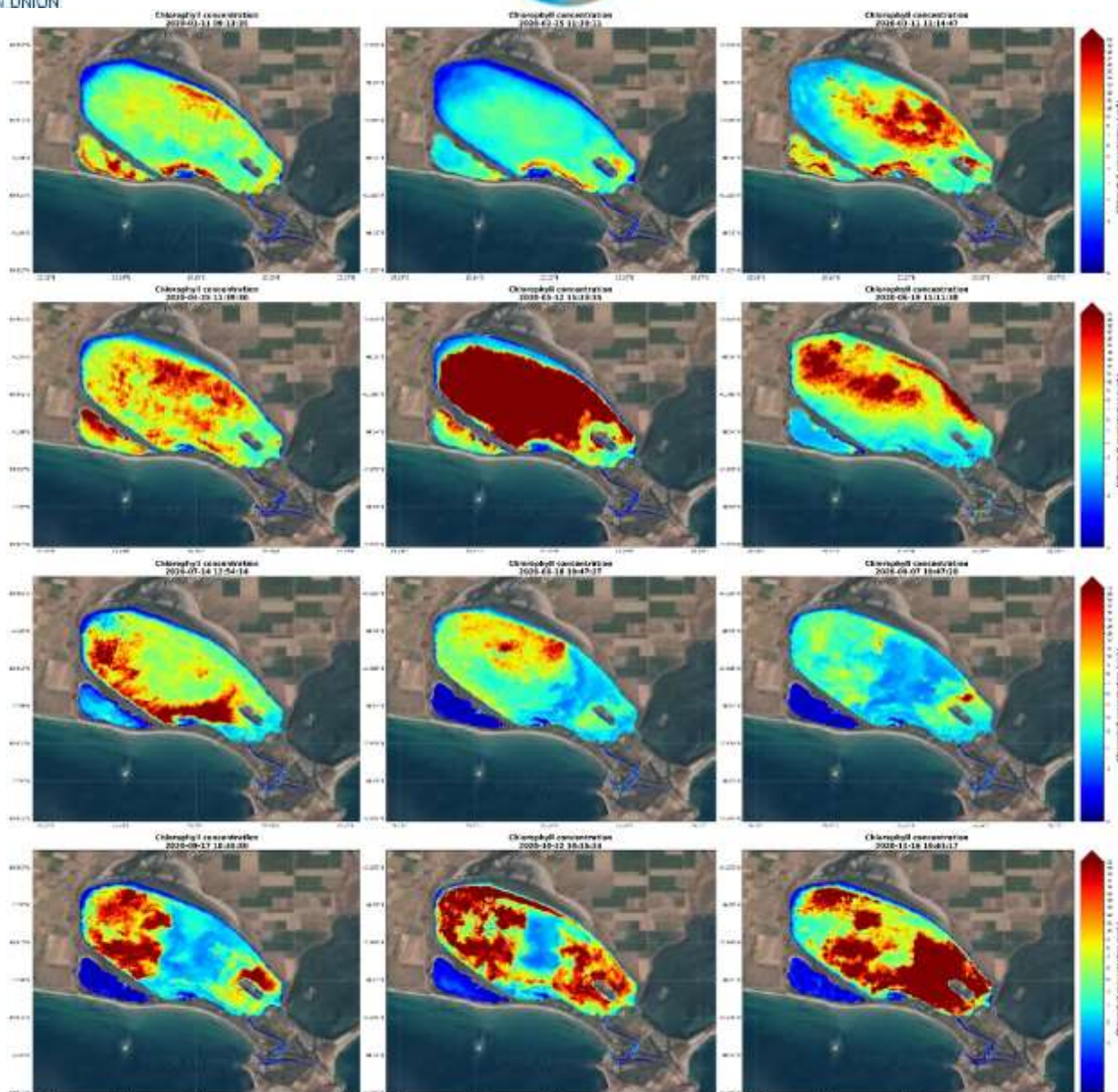


Figure 73. Seasonal evolution of Chl-a concentration in Ptelea lagoon for the year 2020, based on Sentinel 2 satellite images.

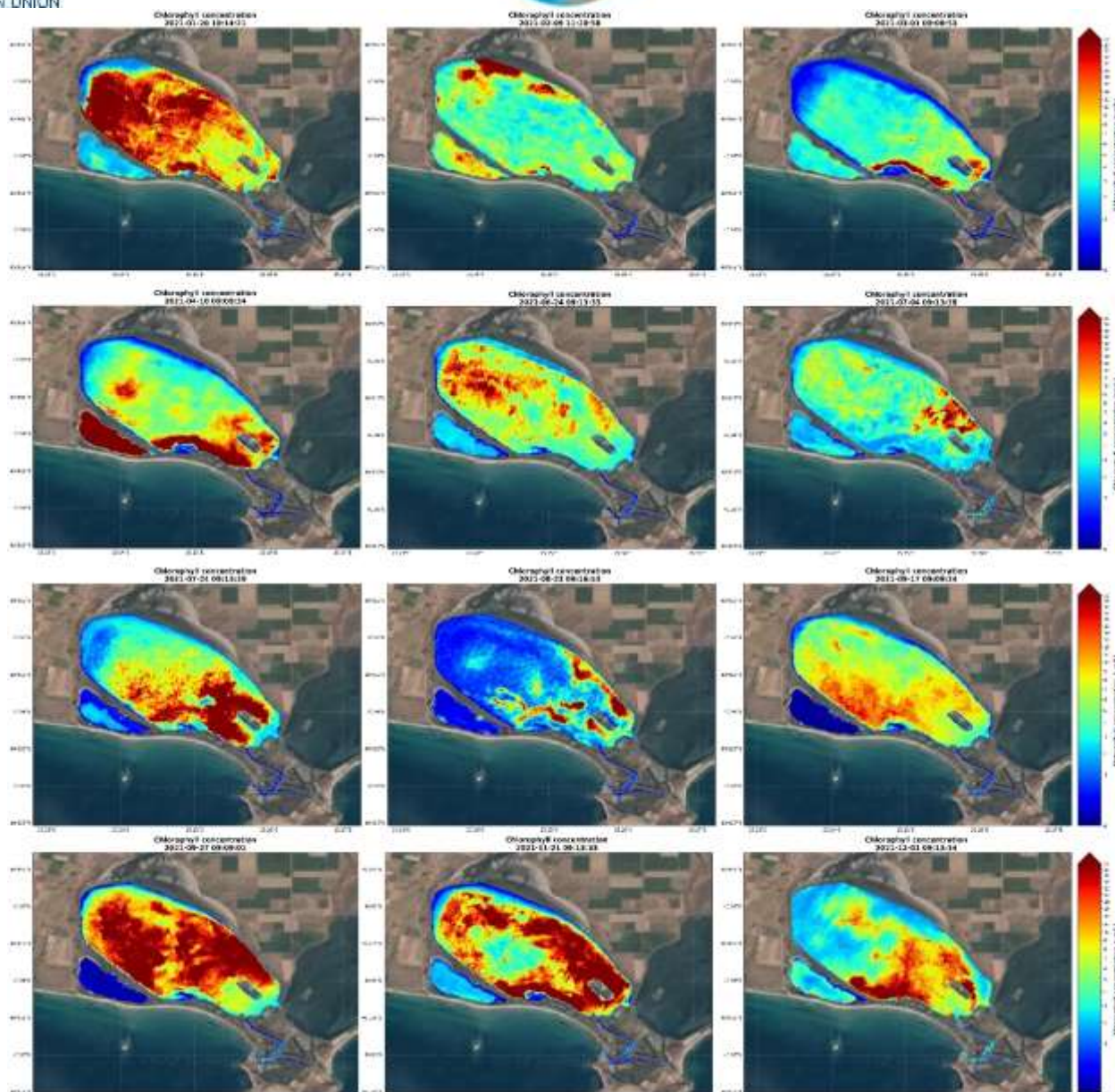


Figure 74. Seasonal evolution of Chl-a concentration in Ptelea lagoon for the year 2021, based on Sentinel 2 satellite images.

## 3.2 Chlorophyll statistical analysis

Satellite-derived Chlorophyll-a data were extracted from specific points (grid cells), representing the eutrophication conditions at sub-basins of the Nestos and Vistonis coastal lagoons. The analysis was divided in two parts: the analysis on the mean-monthly Landsat data and the analysis on the mean-monthly Sentinel data. Daily Chl-a values were monthly-averaged to smooth out any outliers found in data, as a result of the proximity of the cell to land and the impact of water column shallowness.

Data analysis was performed according to the following steps:

- At each point, statistical measures, like the minimum, maximum, median, mean, standard deviation, skewness and kurtosis were computed.
- An initial assessment of the theoretical probability density function (PDF) fitted on the data was given through the construction of the skewness-kurtosis graph (Cullen and Frey, 1999), in which the Chl-a data distribution were plotted against a series of well-known theoretical distributions (normal, exponential, log-normal, gamma, Weibull). The higher the distance among points, the larger the discrepancy among distributions.
- The best-fit theoretical PDF was determined following the AIC and BIC criteria, and its parameters were computed following the maximum likelihood estimation (MLE) method.
- The probability of exceeding the Chl-a concentration threshold of 2  $\mu\text{g/l}$  was assessed.